



Enhanced internal tidal mixing in the Philippine Sea mesoscale environment

Jia You^{1, 3, 4}, Zhenhua Xu^{*1, 2, 3, 4}, Qun Li⁵, Robin Robertson⁶, Peiwen Zhang^{1, 3, 4},
Baoshu Yin^{1, 2, 3, 4}

¹CAS Key Laboratory of Ocean Circulation and Waves, Institute of Oceanology, Chinese Academy of Sciences, Qingdao, China

²Pilot National Laboratory for Marine Science and Technology, Qingdao, China

³Center for Ocean Mega-Science, Chinese Academy of Sciences, Qingdao, China

⁴College of Earth and Planetary Sciences, University of Chinese Academy of Sciences, Beijing, China

⁵Polar Research Institute of China, Shanghai, China

⁶China-Asean College of Marine Science, Xiamen University Malaysia, Sepang, Malaysia

**Corresponding author: Zhenhua Xu, Institute of Oceanology, Chinese Academy of Sciences; Email: xuzhenhua@qdio.ac.cn.*

Abstract.

Turbulent mixing in the ocean interior is mainly contributed by internal wave breaking; however, the mixing properties and the modulation effects of mesoscale environmental factors are not well-known. Here, the spatially inhomogeneous and seasonally variable diapycnal diffusivities in the upper Philippine Sea were estimated from ARGO float data using a strain-based finescale parameterization. Based on a coordinated analysis of multi-source data, we found that the driving processes for diapycnal diffusivities mainly included the near-inertial waves and internal tides. Mesoscale features were important in intensifying the mixing and modulating its spatial pattern. One interesting finding was that, besides near-inertial waves, internal tides also contributed significant diapycnal mixing for the upper Philippine Sea. The seasonal cycles of diapycnal diffusivities and their contributors differed zonally. In the mid-latitudes, wind-mixing dominated and was strongest in winter and weakest in summer. In contrast, tidal-mixing was more predominant in the lower-latitudes and had no apparent seasonal variability. Furthermore, we provide evidence that the mesoscale environment in the Philippine Sea played a significant role in regulating the intensity and shaping the spatial inhomogeneity of the internal tidal mixing. The magnitudes of internal tidal mixing was greatly elevated in regions of energetic mesoscale processes. The anticyclonic mesoscale features were found to enhance diapycnal mixing more significantly than did cyclonic ones.

Keywords: Mixing, Internal tides, Mesoscale, the Philippine Sea



1. Introduction

Turbulent mixing can alter both the horizontal and vertical distributions of temperature and salinity gradients. These then modulate the ocean circulation variability, both globally and regionally. Many studies have shown the existence of a complicated spatiotemporal pattern of diapycnal mixing in the ocean interior. Such mixing inhomogeneity can influence the hydrological characteristics, ocean circulation variability and climate change. The breaking of internal waves is believed to be the main contributor to the ocean's diapycnal mixing (eg. Liu et al., 2013, Robertson R., 2001). Thus, clear understanding the spatial patterns and dissipation processes of broad-band internal waves is necessary to clarify and depict the global ocean mixing climatology.

The long-wavelength internal waves in the ocean are mainly in the form of near-inertial internal waves (NIWs) and internal tides (eg. Alford and Gregg, 2001; Cao et al., 2018; Klymak et al., 2006), and the internal solitary waves evolved from them also can trigger mixing (eg. Deepwell et al., 2017; Grimshaw, et al., 2010; Shen et al., 2020). The wind-input NIW energy to the mixing layer is about 0.3-1.4 TW (eg. Alford, 2003; Liu et al., 2017; Rimac et al., 2013; Watanabe and Hibiya, 2002). The NIW energy propagate downward, mainly dissipate and drive energetic mixing within the upper ocean (Wunsch and Ferrari, 2004). Barotropic tidal currents flowing over rough topographic features can generate internal tides (eg. Robertson R., 2001), with the global energy of 1.0 TW (Egbert and Ray, 2001; Jayne and St. Laurent, 2001; Song and Chen, 2020). Near the sources, the internal tidal mixing intensify above the bathymetries, meanwhile, in the remote area, the tidal mixing is distributed throughout the water column due to the multiple reflection and refraction processes. Therefore, the relative contributions to the upper-layer diapycnal diffusivities by NIWs and internal tides should differ regionally, which deserves further investigation.

In mid-latitudes, NIWs dominated the upper ocean mixing, as a result of the presence of westerlies and frequent storms (eg. Alford et al., 2016; Jing et al., 2011; Whalen et al., 2018). However, from the global view, the upper ocean mixing geography is inconsistent with the global wind field distribution. For example, in low-latitudes, upper ocean mixing hotspots are located nearer to rough topographic features, regardless of the wind conditions. This indicates that upper ocean mixing might be attributed to non-wind-driven internal waves, such as internal tides. In order to better understand the ocean mixing patterns and modulation mechanisms, we need to clarify the relative contributions between the



62 wind and tidal energy.

63 Internal tides are generally considered to be important to ocean mixing in the deep ocean, beyond the
64 influence of winds (Ferrari and Wunsch, 2009; Munk et al., 1998; MacKinnon et al., 2017). Many
65 factors influence the spatial pattern and energy transfer of internal tides. Higher-mode internal tides
66 break more easily near their sources, while the low-mode internal tides propagate long distances, even
67 thousands of kilometers. Propagating internal tides will be limited by several factors, such as
68 topography, stratification and turning latitude (eg. Vlasenko et al., 2013; Song and Chen, 2020;
69 Hazewinkel & Winters, 2011). Wave-wave interaction in the ocean also influences the spatiotemporal
70 variability of internal tides. For example, PSI (parametric subharmonic instability) is a potential avenue
71 to transfer internal tidal energy to other frequencies (Ansong et al., 2018). Moreover, stratification and
72 background flows also contribute to internal tidal spatial and temporal variability (eg. Karry et al., 2016;
73 Huang et al., 2018; Chang et al., 2019). Due to the complicated multi-scales of the background flows, it
74 is still unclear about how the background flow modulates the internal tides, their energy dissipation and
75 ocean mixing.

76 Recent research suggests that the mesoscale environment is a key factor influencing ocean mixing.
77 There is evidence that mesoscale eddies can enhance wind-driven mixing and internal tidal dissipation.
78 This enhancement will be more significant in the presence of an anticyclonic eddy (eg. Jing et al., 2011;
79 Whalen et al., 2018). Likewise, regional studies indicate that mesoscale features modulate the
80 generation and propagation of internal tides. Mesoscale currents can also broaden the range undergoing
81 internal tide critical latitude effects and enhance the energy transfer from diurnal frequencies to
82 semidiurnal or high frequencies (Dong et al., 2019). Mesoscale eddies are found to modulate internal
83 tide propagation (Rainville and Pinkel, 2006; Park and Watts, 2006; Zhao et al., 2010) and enable the
84 internal tide to lose its coherence (Nash et al., 2012; Kerry et al., 2016; Ponte and Klein, 2015).
85 Numerical simulation results support these observations (Kerry et al. 2014), indicating that the patterns
86 of internal tides is largely modulated by the position of eddies. An idealized numerical experiment
87 shows that the energy of internal tides shows bundled beams after passing through an eddy (Dunphy
88 and Lamb, 2014). And the mode-1 internal tides interactions with eddies will trigger higher-mode
89 signals. Up to now, research about mesoscale–internal tide interactions has been primarily focused on
90 the propagation pattern or 3-D structure of internal tides and has ignored their energy dissipation and



91 mixing effects. The latter is more important for altering the ocean circulation variability and climate
92 change.

93 The Philippine Sea, located in the Northwestern Pacific Ocean, is one of the most energetic internal
94 tidal regimes in the world. In this region, powerful internal tides significantly enhance ocean mixing, as
95 shown by numerical simulations (Wang et al., 2018). The importance of sub-inertial shear to ocean
96 mixing has been hypothesized from observations (Zhang et al., 2019), and the importance of internal
97 tides to mixing is supported through parameterization techniques (Qiu et al., 2012). On the other hand,
98 the Philippine Sea is an area with frequent typhoons, which make significant contributions to ocean
99 mixing. Multiple factors and mechanisms impact the turbulent mixing distribution in the Philippine Sea
100 (Wang et al., 2018). To date, it is unclear what the dominant factors are and how these factors modulate
101 the ocean mixing properties. Moreover, the role of mesoscale environment in regulating ocean mixing
102 is still not well understood.

103 At present, coupled numerical models are basically able to accurately simulate the generation and
104 propagation of internal tides. The internal tide dissipation and induced mixing are found to be
105 important for the determination of correct mixing parameterizations in numerical models (Robertson
106 and Dong, 2019). Some existing studies focus on the simulations of internal tidal breaking and tidally
107 induced mixing (Kerry et al., 2013; Kerry et al., 2014; Muller, 2013; Wang et al., 2018). It is difficult to
108 provide a complete spatial and temporal picture from direct observations of turbulence. This is due to
109 the scarcity of observations and their patchy distribution in time and space. Multisource data covering
110 multiple tidal cycles or preferably a spring-neap cycle, as well as a broad domain, are necessary to
111 acquire the spatiotemporal distribution and few of these have been collected. The development and
112 application of parameterization methods provide greater possibility of characterizing a broad-regional
113 mixing distribution and variability. A global pattern of ocean mixing has been provided using these
114 parameterization methods (Whalen et al. 2012; Kunze 2017). Furthermore, sensitivity studies have
115 been performed investigating the dependence of several factors to global mixing, such as bottom
116 roughness, internal tides, wind and background flows (eg. Whalen et al. 2012; Waterhouse. 2014;
117 Kunze and Eric. 2017; Whalen et al. 2018; Zhang et al. 2019). At present, parameterization is the most
118 effective method to investigate the modulation of tidal mixing by mesoscale background flows.

119 The spatial pattern and temporal variability of diapycnal diffusivities in the Philippine Sea are
120 examined in this paper. We provide evidence to verify the importance of tidal mixing in the upper layer



of this region. Moreover, we illustrate the modulation of mesoscale environment in tidal mixing properties and distributions. Our data and methods are detailed in Section 2. Results and analysis, including the spatial patterns and seasonal cycle of mixing, contributions of influencing factors and internal tide-mesoscale interrelationships, are shown in Section 3. Finally the summary and discussion are given in Section 4.

2. Method and Data

2.1 ARGO and Fine-scale parameterization method

The ARGO Program is a joint international effort involving more than 30 countries and organizations and having deployed over 15,000 freely drifting floats since 2000. The accumulated total collected profiles exceeds 2 million profiles of conductivity, temperature, depth (CTD) along with other geobiochemical parameters. The ARGO program has become the main data source for many research and operational predictions of oceanography and atmospheric science (<http://www.ARGU.ucsd.edu>). We screened the profiles from the Philippines Sea with quality control and estimated diapycnal diffusivity and dissipation rate from them using a finescale parameterization.

The diapycnal diffusivity and turbulent kinetic energy dissipation rate can be estimated from a fine-scale strain structure. This is based on a hypothesis that the energy can be transported from large to small scales. In such scales, waves break due to shear or convective instabilities by weakly nonlinear interactions between internal waves (Kunze et al., 2006). Presently, this method has been widely used for the global ocean (eg. Wu et al., 2011; Kunze et al., 2017; Whalen et al., 2012; Fer et al., 2010; Waterhouse et al., 2014). The dissipation rate ε can be expressed as

$$\varepsilon = \varepsilon_0 \frac{\overline{N^2} \langle \xi_z^2 \rangle^2}{N_0^2 \langle \xi_{zGM}^2 \rangle^2} h(R_\omega) L(f, \overline{N}) \quad (1)$$

where $\varepsilon_0 = 6.73 \times 10^{-10} W/kg$ and $N_0 = 5.24 \times 10^{-3}/s$, and $\overline{N^2}$ represents the averaged buoyancy frequency of the segment. $\langle \xi_{zGM}^2 \rangle$ and $\langle \xi_z^2 \rangle$ are strain variance from the Garrett-Munk (GM) spectrum (Gregg and Kunze, 1991) and the observed strain variance, respectively. The angle brackets indicate integration over a specified range of vertical internal wavenumbers (see equations 4 and 5). The function $h(R_\omega)$ accounts for the frequency content of the internal wave field and R_ω represents shear/strain variance ratio. R_ω is fixed at 7, which is a global mean value (Kunze et al., 2006).

$$h(R_\omega) = \frac{1}{6\sqrt{2}} \frac{R_\omega(R_\omega+1)}{\sqrt{R_\omega-1}} \quad (2)$$



149 The function $L(f, \bar{N})$ corrects for a latitudinal dependence, here f is the local Coriolis frequency,
 150 and f_{30} is the Coriolis frequency at 30° , and \bar{N} is the vertically averaged buoyancy frequency of the
 151 segment.

$$152 \quad L(f, \bar{N}) = \frac{f \operatorname{acrcosh}(\frac{\bar{N}}{f})}{f_{30} \operatorname{acrcosh}(\frac{\bar{N}}{f_{30}})} \quad (3)$$

153 strain ξ_z was calculated from each segment,

$$154 \quad \xi_z = \frac{N^2 - N_{ref}^2}{N^2} \quad (4)$$

$$155 \quad \langle \xi_z^2 \rangle = \int_{k_{min}}^{k_{max}} S_{str}(k_z) dk_z \leq 0.2 \quad (5)$$

156 We derived N from 2 to 10 dbar-processed temperature, salinity, and pressure data according to the
 157 ARGO float resolution. N_{ref} , as a smooth piece-wise quadratic fit to the observed N profile, is fitted to
 158 24 m. Here we remove segments that vary in the range of $\langle N^2 \rangle > 5 \times 10^{-4} s^{-2}$ or $\langle N^2 \rangle < 1 \times$
 159 $10^{-9} s^{-2}$ since the strain signal at these levels is dominated by noise (Whalen et al., 2018). By
 160 applying a fast Fourier transform (FFT) on half-overlapping 256 m segments along each vertical ξ_z
 161 profile, we computed the spectra $S_{str}(k_z)$ and integrated them to determine the strain variance. We
 162 integrated these spectra between the vertical wavenumbers $k_{min} = 0.003 \text{ cmp}$ and $k_{max} =$
 163 0.02 cmp according to global internal tide typical scales and equation 5, respectively. Substituting
 164 $\langle \xi_z^2 \rangle$ into equation (1) ultimately yields 32 m resolved vertical profiles of each observed profiles. The
 165 dissipation rate ε is related to the diapycnal diffusivity K_z by the Osborn relation

$$166 \quad K_z = \Gamma \frac{\varepsilon}{N^2} \quad (6)$$

167 where the flux coefficient Γ is fixed at 0.2 generally.

168

169 2.2 ERA-Interim and Slab-model

170 The near-inertial energy flux for each observation profile was calculated using the 10 m wind speed
 171 product from ERA-Interim (<https://www.ecmwf.int/en/forecasts/datasets>), which is 6-hourly wind
 172 speed on a grid of $0.75^\circ \times 0.75^\circ$. We selected the mean near-inertial flux of 30-50 days before the
 173 time of each diapycnal diffusivity estimation as our measure of the near-inertial flux, with the
 174 consideration of the propagation of NIWs.

175 The wind-drive NIW energy flux can be directly estimated using a slab model, which assumes that



the inertial oscillations in the mixed layer do not interact with the background fields. The mixed layer current velocity can be described by

$$\frac{dZ}{dt} + (r + if)Z = \frac{T}{\rho H} \quad (7)$$

where $Z = u + iv$ is the mixed layer oscillating component of full current, and i is an imaginary number to indicate the latitudinal component. $T = (\tau_x + i\tau_y)$ is the wind stress on the sea surface, f is the local Coriolis parameter, r is the frequency-dependent damping parameter, which was fixed at $0.15 f$ for these calculations. ρ is sea water density and fixed at 1024 kg/m^3 . H is the mixed-layer depth and was set to a constant 25 m. We can calculate the oscillating component of full velocity from equation 7 and obtain the near-inertial component through a bandpass filter of $[0.85, 1.25] f$. The near-inertial energy flux is calculated as

$$H(\Pi) = \text{Re}(Z \cdot T^*) \quad (8)$$

the asterisk (*) indicates the complex conjugate of a variable.

2.3 AVISO and Eddy kinetic energy

The eddy kinetic energy is estimated based on geostrophic calculation as:

$$EKE = \frac{1}{2} (U_g'^2 + V_g'^2) \quad (9)$$

$$U_g' = -\frac{g}{f} \frac{\Delta \eta'}{\Delta y} \quad V_g' = -\frac{g}{f} \frac{\Delta \eta'}{\Delta x} \quad (10)$$

where U_g' and V_g' are the geostrophic velocities in the east-west and north-south directions, respectively. They are taken from the AVISO (<http://www.aviso.altimetry.fr/duacs/>) geostrophic velocity product. η' indicates sea level anomaly (SLA).

2.4 Internal tidal conversion rates

The internal tidal conversion rate was provided by SEANOE (<https://www.seanoe.org/data/>, C.de Lavergne et al., 2019), including 8 main tidal constituents. We used the mode-summed internal tidal conversion rates of M_2 and K_1 , and integrated 8 main tidal constituents in present study.

3. Results

3.1 Spatial pattern of diapycnal mixing in the upper Philippine Sea

The diapycnal diffusivities were used as indicators of ocean diapycnal mixing. The pattern averaged within 250-500 m is shown in Fig.1a. The K_z was estimated from the ARGO profiles, with an average



on each cell of $0.5^\circ \times 0.5^\circ$. The magnitude of diapycnal diffusivities increased with latitude, reaching $10^{-4} \text{ m}^2 \text{ s}^{-1}$ in the northern part of this area (30°N – 36°N). The mean value of K_z was about $\text{O}(-6)$ – $\text{O}(-5)$ in lower latitude. While, it was remarkable that the magnitude of K_z also increased significantly in some low-latitude regions, reaching $\text{O}(-4)$ or higher. These regions include Izu Ridge (Nagasawa et al., 2005; Tanaka et al., 2018) and Luzon Strait. Reviewing the influence of topography, wind and internal tide (Fig.1b-d) on ocean mixing, it was found that the zonal variability of K_z was consistent with the wind intensity distribution. Upper ocean mixing was significantly enhanced at mid-latitudes due to the presence of westerlies. In addition, K_z was also enhanced near several key internal tide sources, such as the Luzon Strait, Bonin Ridge, Izu Ridge, Dadong Ridge, etc. At these sites, the magnitude of K_z was obviously larger than other areas at the same latitude, indicating a significant role of internal tides. Additionally, the enhancement of deep ocean mixing at these sites was even more obvious (not shown).

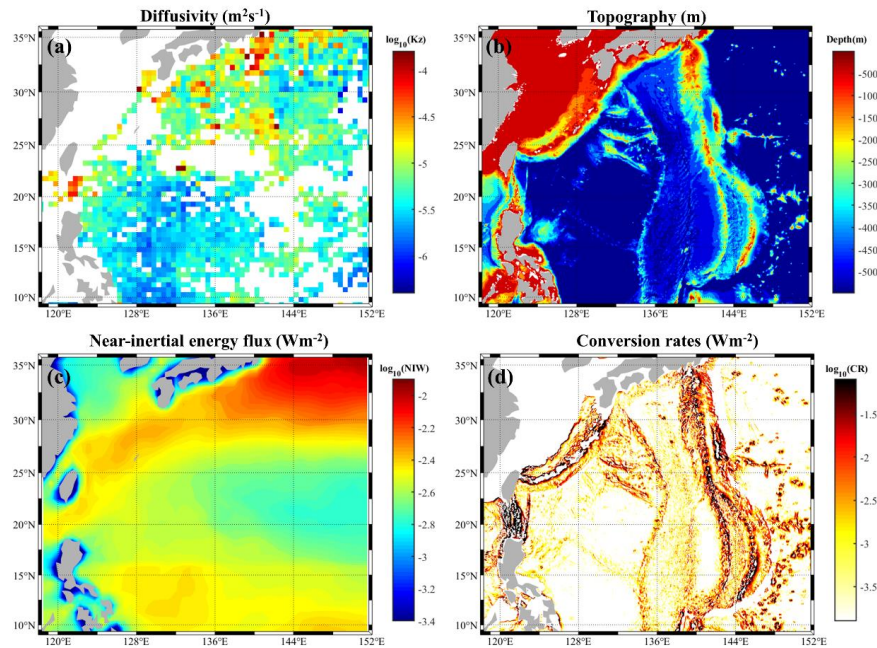
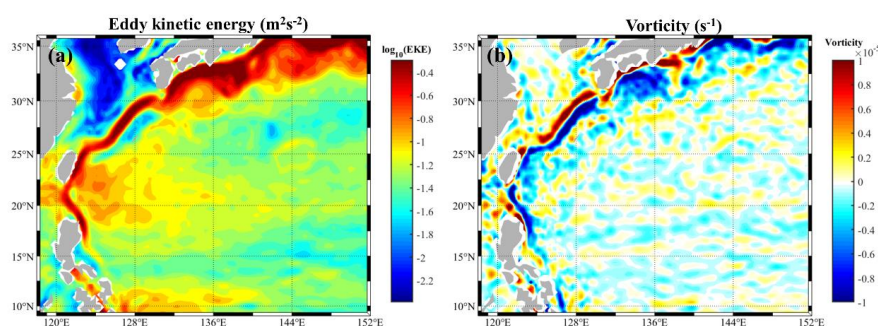


Figure 1 Maps of (a) log-scale averaged diapycnal diffusivities K_z ($\text{m}^2 \text{s}^{-1}$) estimated from ARGO profiles, (b) topography, (c) log-scale long-term averaged near-inertial energy flux from wind (Wm^{-2}), and (d) log-scale M2 internal tide conversion rates (Wm^{-2}).

It can be noted that the pattern of diapycnal diffusivities was not completely consistent with those of either internal tides or winds. This suggests that the ocean mixing was modulated by other factors than



221 tides and winds. The magnitudes of K_z also vary for internal tide source sites. Considering that the
 222 Philippine Sea is a region with energetic mesoscale motions (Fig.2), the influences of mesoscale
 223 features in turbulent mixing should be taken into account. The existence of mesoscale features can alter
 224 the propagation and dissipation of internal tides. Therefore, the Philippine Sea is an ideal region to
 225 study the modulation of background flows on turbulent mixing associated with strong internal tides.



226
 227 **Figure 2** Maps of (a) log-scale long-term averaged eddy kinetic energy and (b) long-term averaged vorticity.

229 3.2 Seasonal variability of mixing at different latitudes

230 The seasonal cycle for diapycnal diffusivities also differs zonally. Here, we divided the Philippine
 231 Sea into two portions: low-latitude (10°N-25°N) and mid-latitude (25°N-35°N). The diapycnal
 232 diffusivities K_z were averaged in each latitude band (Fig.3). At the depth of 250-500 m in the
 233 mid-latitude, the diapycnal diffusivities had a significant seasonal trend as strong in winter and weak in
 234 summer. This is consistent with the seasonal fluctuation of near-inertial energy from wind. Such a
 235 seasonal cycle could also be found at 500-1000 m and 1000-1500 m in the mid-latitudes, but it was
 236 relatively weaker, especially after 2016. In the lower latitudes, the NIW energy was still strong in
 237 winter and weak in summer, but a seasonal dependence of turbulent mixing was not obvious, even in
 238 the upper ocean. Consequently, the wind was found to play a significant role in driving turbulent
 239 mixing at mid-latitude, but was insignificant at low latitudes. Other factors drove and modulated
 240 turbulent mixing in low latitudes.

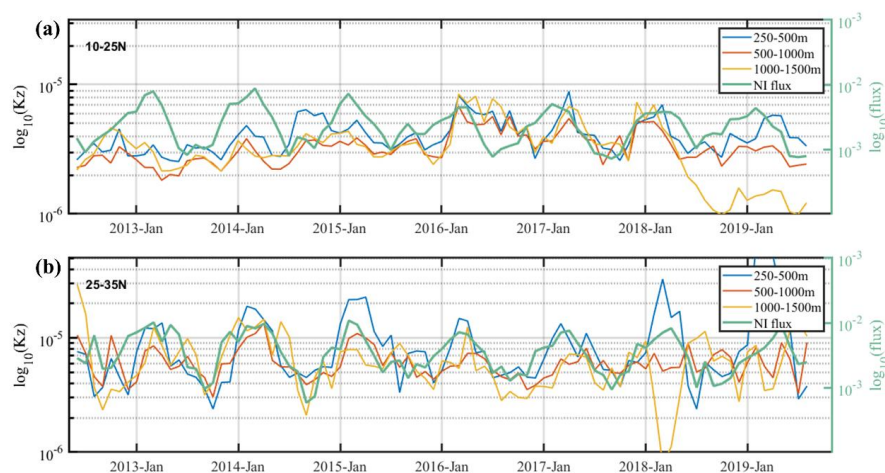


Figure 3 Seasonal cycles in diapycnal diffusivities (colorful line) and near-inertial energy flux from wind (green) extends to 250-500 m, 500-1000 m and 1000-1500 m in (a) 10°N -25°N and (b) 25°N -35°N, which is averaged in each month and all water column.

3.3 Impact factors

3.3.1 Relative contributions

The turbulent mixing of the Philippine Sea displayed an obvious zonal dependence, so the latitudinal influence was examined for several factors: internal tides, wind and eddy kinetic energy (Fig.4). The rates of diapycnal diffusivities in regions of weak/strong internal tides, weak/strong NIW energy, and high/low eddy kinetic energy were calculated in each 1° latitude, respectively. If the rate was close to 1, the influence of this factor was insignificant, while a larger rate indicated a greater contribution.

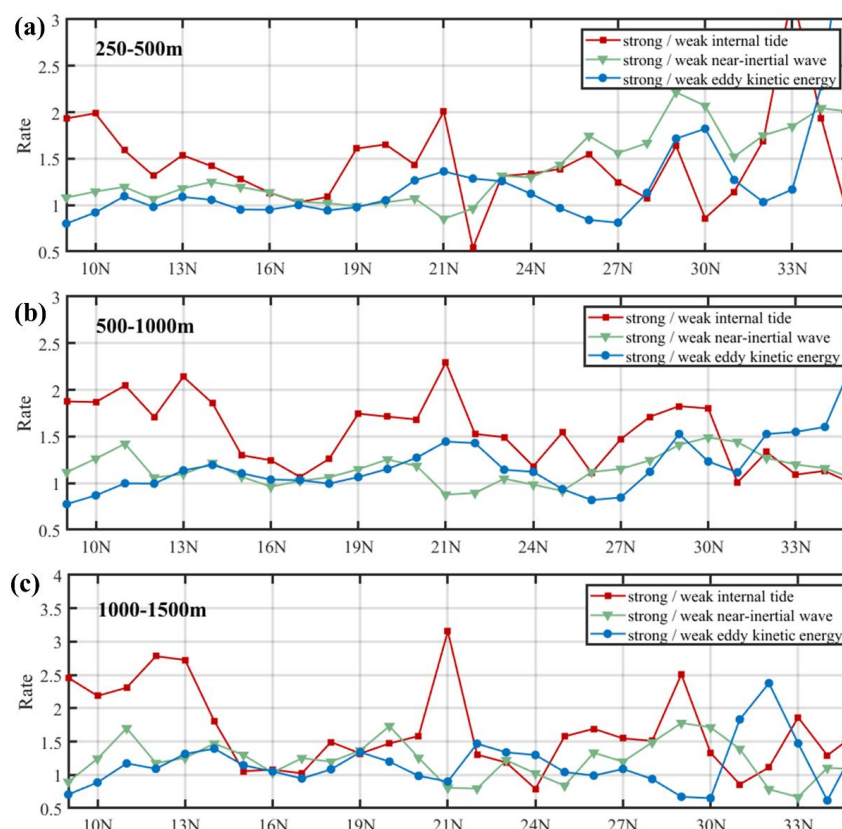


Figure 4 Rates of diapycnal diffusivities between areas over strong (greater than median) and weak internal tide (red lines), strong (greater than median) and weak near-inertial wave (green lines) and strong (greater than median) and weak eddy kinetic energy (blue lines) for each 1° latitude bands in the depth range of (a) 250-500 m, (b) 500-1000 m and (c) 1000-1500 m, Which averages for each bands containing more than 10 estimates.

At depths of 250-500 m, the rate associated with internal tide increased significantly at 10°N, 21°N and 33°N. These latitudes correspond to Guap seamount, Luzon Strait and Izu Ridge, which are main internal tide source sites. It reached 2 near these three latitudes, indicating that strong internal tides triggered the enhancement of K_z twice as much compared to the regions of weak internal tides. In addition, north of 23°N, the rate in related to NIW in the upper ocean increased with latitude. And it exceeded the internal tidal contribution north of 25°N, which indicated that the wind plays a more important role in mixing at this latitude band. Taking the wind as the driving factor better explains the seasonal cycle of diapycnal diffusivities in Fig.3, since the winds have an apparent seasonal



dependence. The obvious seasonal trend of K_z due to the important contribution of wind occurs between 25°N–35°N. In contrast, the rate for wind is ~ 1 at lower latitudes, indicating that the wind-driven mixing is insignificant here with the absence of wind-driven seasonal cycle.

The contribution of wind to turbulent mixing is significantly reduced in the depth ranges of 500–1000 m and 1000–1500 m (Fig.4 b and c). The rate only increased slightly at mid-latitudes, less than 2 anywhere. In contrast, the enhancement of mixing triggered by internal tides at these depth ranges was more significant, with the rates exceeding 3.5 at some latitudes. This suggested that internal tides played a more important role in deep ocean mixing. Furthermore, internal tides significantly enhanced K_z around 13°N, 21°N, and 29°N, corresponding to the sources of Mariana Trench, Luzon Strait and Bonin Ridge, respectively. Such enhancement was not obvious at the Izu Ridge possibly due to the shallower depth and paucity of deep data, or the turning latitude effects in this area.

Combined with the analysis of relative contributions of different factors in different layers, it was concluded that the contribution of internal tides in turbulent mixing is more important in low latitudes of the Philippine Sea. In this area, the wind and mesoscale features did not significantly enhance K_z . At mid-latitudes, internal tides still played an important role, but the wind contribution was more significant in the upper ocean. The wind drove turbulent mixing even at the depths of 500–1000 m and 1000–1500 m. The mid-latitude region not only corresponds to westerlies, but also features energetic mesoscale motions. Therefore, the mesoscale features might be a potential factor for the enhanced turbulent mixing.

In the low latitudes, K_z did not increase in the regions of high eddy kinetic energy or strong near-inertial energy, whereas, it increased significantly in the regions of strong internal tides. This enhancement was more obvious below 400 m (Fig.5 a). And in the mid-latitudes, K_z in the upper ocean increased significantly corresponding to strong winds with compared to weak winds (Fig.5 b). Meanwhile, K_z was also larger in the regions of strong internal tides and high EKE in the upper ocean. The enhancement of wind or EKE to turbulent mixing significantly weakened below 600 m, while the enhancement of internal tides increased with depth. This indicates that internal tides played a significant role in turbulent mixing not only in the low latitudes, but also in the mid latitudes with their strong winds.

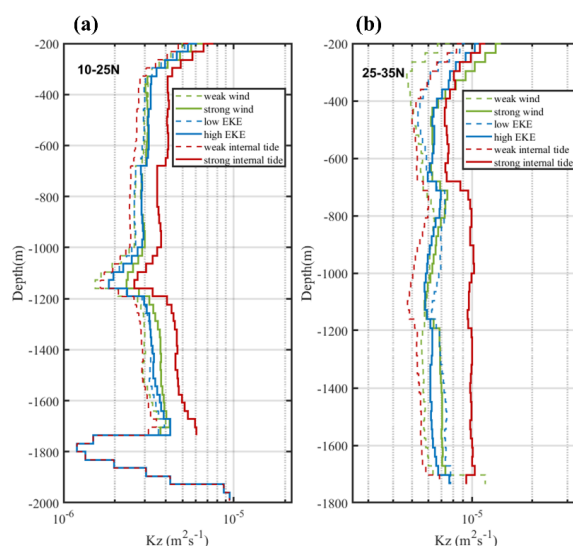


Figure 5 Vertical structures of geometric averaged diapycnal diffusivities K_z with weak and strong wind (green), low and high EKE (blue) and weak and strong internal tide (red) in the (a) low-latitude and (b) middle latitudes.

3.3.2 Wind

The least squares linear fit slopes of K_z to NIW energy from wind represent the mixing response to wind. Here, the Philippine Sea is divided into 10°N–15°N, 15°N–25°N and 25°N–35°N (Fig.6). At the depth of 250–500 m, the slope is the largest in 25°N–35°N (~0.305), followed by that in 10°N–15°N (~0.133), and the smallest in 15°N–25°N (~0.013). The wind driven turbulent mixing was most significant between 25°N–35°N, but was insignificant between 15°N–25°N. At the depth of 500–1000 m, the wind influence on turbulent mixing was weakened in the mid-latitudes. This was consistent with the results of Fig.3 and Fig.4. It proved that the contribution of wind has a zonal dependence, which was significant at the mid-latitudes, but insignificant at low latitudes. In addition, the response of turbulent mixing to wind weakened quickly with depth, indicating that the dominant factor of mixing in the deeper water column was not wind. Accordingly, it was difficult for wind to drive mixing below 1000 m, so we do not show the results at the depth of 1000–1500 m (Fig.4).

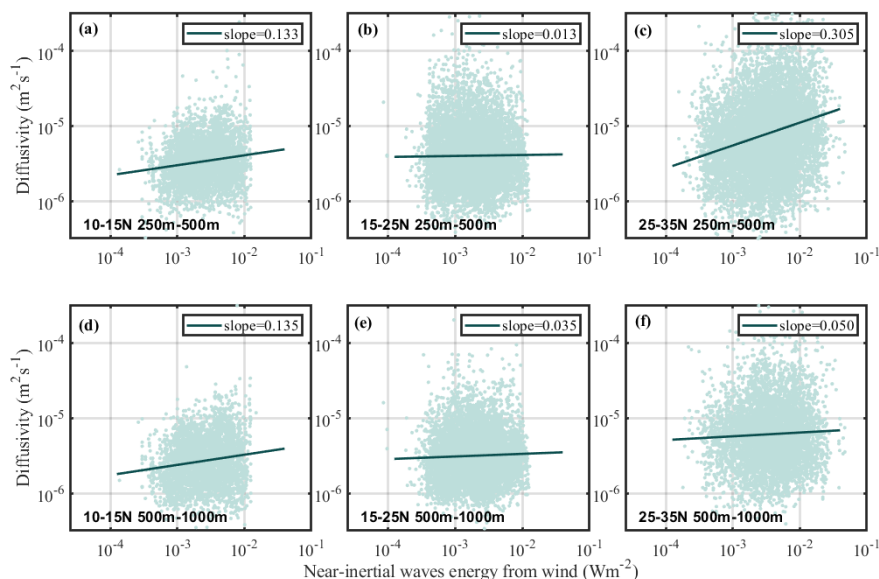


Figure 6 Scatter of log-scale K_z versus log-scale near-inertial energy flux from wind in 250-500 m between (a) 10°N -15°N, (b) 15°N-25°N and (c) 25°N-35°N, and in 500-1000 m between (d) 10°N-15°N, (e) 15°N-25°N and (f) 25°N-35°N. The best-fit slopes are denoted by the solid line.

3.3.3 Tide

The slopes of K_z to internal tides conversion rates represent the mixing response to internal tides. As discussed above, the mixing significantly responded to the internal tides over the entire Philippine Sea (Fig.7). The relationship was depth dependent. The slopes did not reach 0.1 at the depth of 250-500 m, but increased significantly at 500-1000 m and 1000-1500 m, and exceed 0.13 for the deepest depth band. The response of mixing to internal tides was more significant in the deeper ocean. Focusing on different latitude bands, the slopes of K_z to internal tides is smaller at mid-latitudes. This is because the wind contribution increased in this region, which led to a weakening relative contribution of internal tides. Compared with the internal tide conversion rates, the pattern of K_z was inconsistent with internal tides, even at lower latitudes. It can be inferred that the turbulent mixing was not only affected by the internal tides, but also by other factors. There is a strong western boundary flow, Kuroshio, and an active mesoscale environment in this region. Some researchers have shown that the existence of mesoscale environment will alter the internal tide features, so we reasonably infer that the tidal induced turbulent mixing in this area was modulated by the mesoscale features.

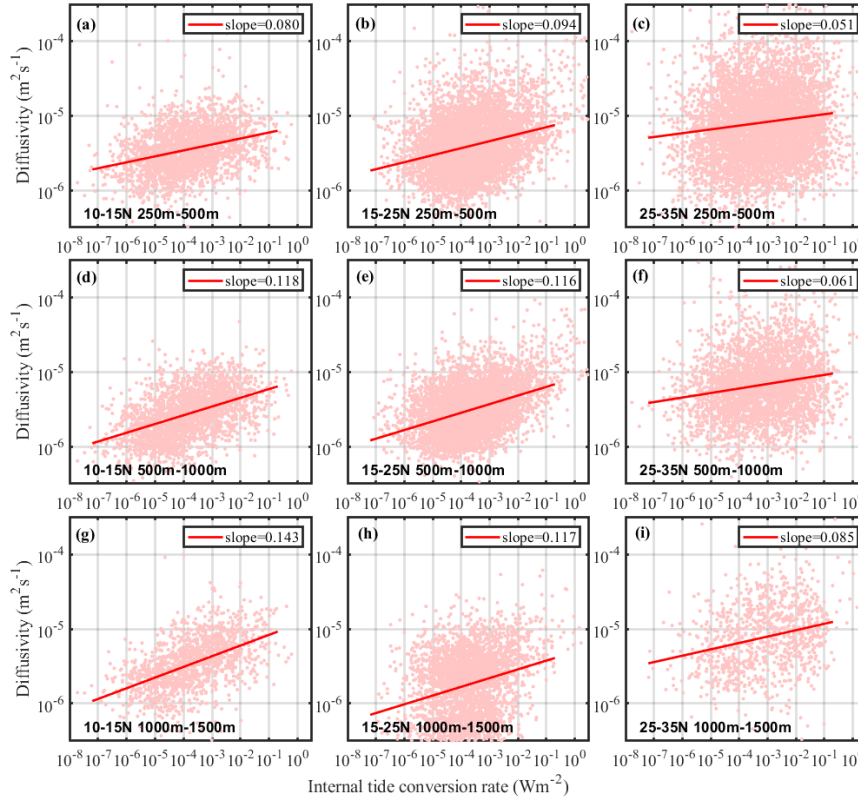


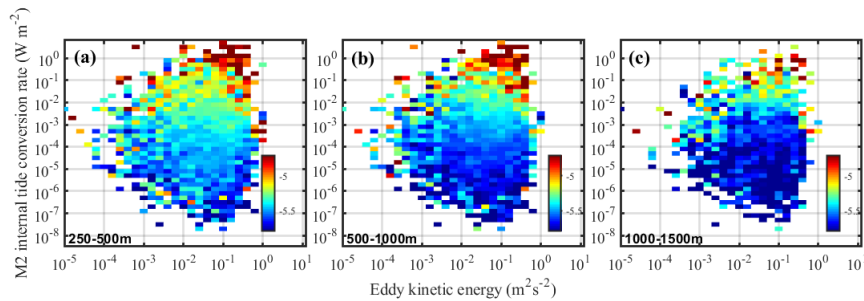
Figure 7 Scatter of log-scale K_z versus log-scale internal tide conversion rate in 250-500 m (row 1), 500-1000 m (row 2), 1000-1500 m (row 3) and the best-fit slopes are denoted by the red line. Columns 1,2,3 are 10°N-15°N, 15°N-25°N and 25°N-35°N latitude bands, respectively.

3.4 Role of Mesoscale features in tidal mixing

Focusing on the low latitudes, where tidal mixing is dominated, the diapycnal diffusivities, K_z , related to internal tides and eddy kinetic energy are shown (Fig.8). The combined influences of mesoscale features and internal tides on mixing are indicated. The increasing internal tide conversion rates significantly enhanced turbulent mixing. When the conversion rate was 10^{-3} Wm^{-2} , the magnitudes of K_z were about $3 \times 10^{-6} \text{ m}^2 \text{ s}^{-1}$, $3 \times 10^{-6} \text{ m}^2 \text{ s}^{-1}$, $1 \times 10^{-6} \text{ m}^2 \text{ s}^{-1}$ at the depth of 250-500 m, 500-1000 m and 1000-1500 m, respectively. When the internal tide conversion rates reached O(-1)-O(0), K_z reached $10^{-5} \text{ m}^2 \text{ s}^{-1}$ at both depths of 250-500 m and 500-1000 m, even exceed $10^{-4} \text{ m}^2 \text{ s}^{-1}$ at some internal tide source sites. In addition, there was a positive correlation between eddy kinetic energy and



346 diapycnal diffusivities. A higher eddy kinetic energy can further increase K_z under the same magnitude
 347 of internal tide conversion rate. Such enhancement was more significant with strong internal tide
 348 conversion rates greater than 10^{-3} W m^{-2} .



349
 350 **Figure 8** Averaged diapycnal diffusivities as a function of EKE and internal tide conversion rates between (a)
 351 250-500 m, (b) 350-500 m and (c) 500-1000 m.

352
 353 M_2 and K_1 tidal constituents were analyzed to clarify the response of K_z to internal tides in the
 354 regions of high eddy kinetic energy (EKE is larger than the regional average value) and low eddy
 355 kinetic energy (Fig.9). The results integrating 8 main tidal constituents (Fig.9 a, b and c) showed that
 356 the slopes in a weak (strong) mesoscale field were smaller (larger), 0.081 (0.105), 0.103(0.134) and
 357 0.103 (0.142) at the depth of 250-500 m, 500-1000 m, 1000-1500 m, respectively. The turbulent mixing
 358 was more sensitive to the internal tide magnitude in the presence of an energetic mesoscale field.
 359 Moreover, such response was more obvious in the region with strong internal tides (such as $>10^{-2} \text{ W m}^{-2}$
 360 conversion rate). In some regions with weak internal tides, such as with internal tide conversion rates
 361 less than 10^{-3} W m^{-2} , the modulation of mesoscale eddies was less significant.

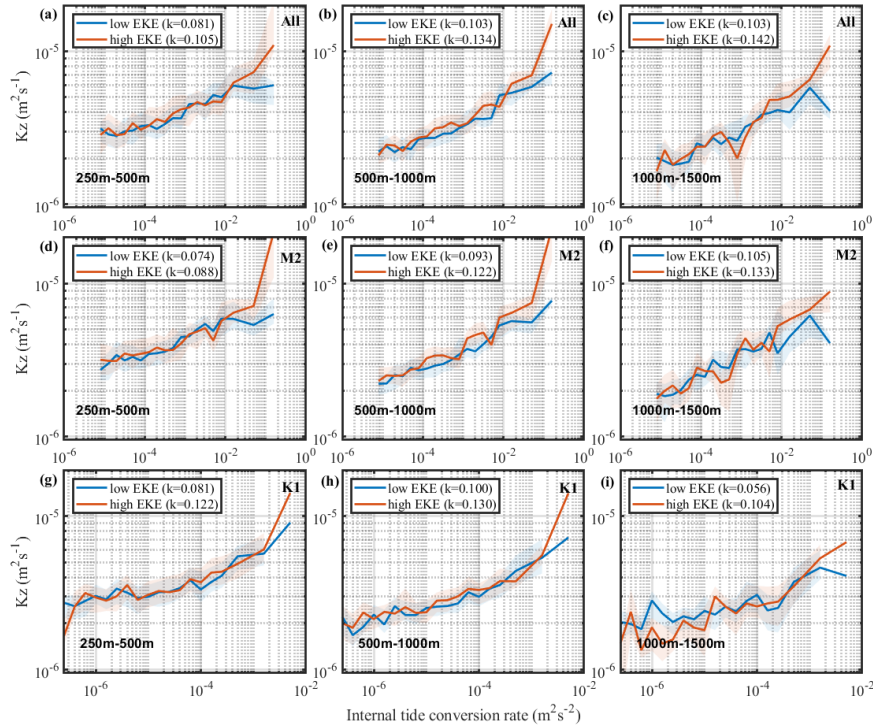


Figure 9 The averaged diffusivity between depths of (a, d, g) 250 m-500 m, (b, e, h) 500 m-1000 m and (c, f, i) 1000 m-1500 m in high (greater than the median) and low (less than the median) eddy kinetic energy. The shade indicate the 1 deviation. Rows 1,2 and 3 are related to 8 main tidal constituents, M_2 internal tide and K_1 internal tide, respectively.

A similar conclusion can be drawn only considering M_2 or K_1 . In regions of high eddy kinetic energy, the change in diffusivities in response to internal tides was significant. And the increase was more sensitive to M_2 internal tide. The enhancement related to M_2 internal tide was more significant below 500 m (Fig.9 d and e), while enhancement of the K_1 internal tide was similar at all depths. This may be due to different features and structures of M_2 and K_1 internal tides. In this area, the modal structure and propagation path of M_2 internal tide are more complicated and more prone to breaking, but those of K_1 were relatively stable. And this area includes the K_1 critical latitude range, which can be broadened by mesoscale currents (Robertson and Dong, 2019).

The modulation of cyclonic and anticyclonic eddies on tidal mixing also differ. The increase of K_z by internal tides in regions with cyclonic eddies ($\text{vorticity} > 3 \times 10^{-6} \text{ s}^{-1}$) and anticyclonic eddies ($\text{vorticity} < -3 \times 10^{-6} \text{ s}^{-1}$) are both shown (Fig.10 and Fig.11). Under the same magnitude of internal tides,



the K_z increase more significantly in the presence of anticyclonic eddies, which is obvious in 250-500 m, and can also be seen in 500-1000 m. Below 1000 m, there is no significant differences between the regions with cyclones and anticyclones.

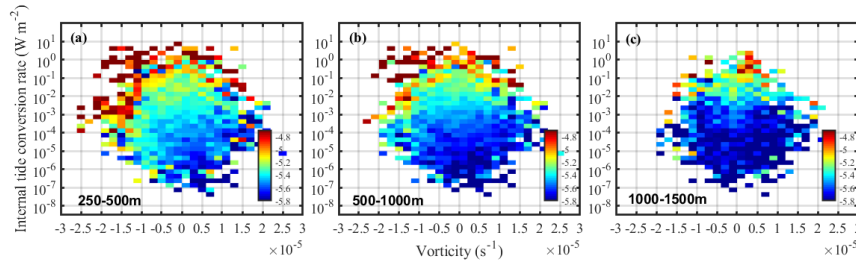


Figure 10 The averaged diapycnal diffusivities as a function of vorticity and internal tides conversion rate between (a) 250-500 m, (b) 500-1000 m and (c) 1000-1500 m

Considering mixing driven by eddies is relatively significant in regions where the tidal mixing is very weak, we only analyze the cases of internal tides conversion rates larger than 10^{-3} W m^{-2} . When the conversion rates become larger than this value, the diapycnal diffusivities at the presence of high eddy kinetic energy increase faster with internal tides (Fig. 9). It was found that the response of turbulent mixing to internal tides was more sensitive in the presence of anticyclones above 1000 m. While below 1000 m, the influence of cyclones is slightly higher than that of anticyclones.

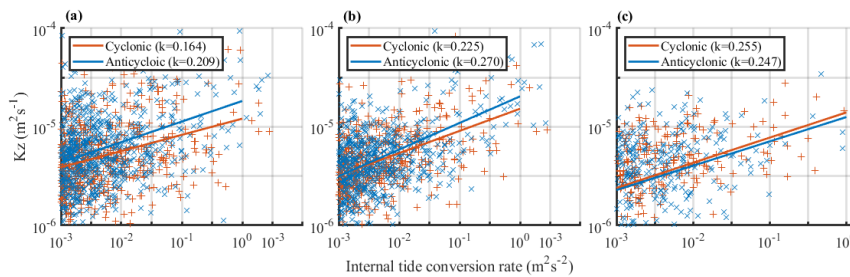


Figure 11 scatter of log-scale K_z versus log-scale internal tide conversion rate with Cyclone (red) and anticyclone (blue) in (a) 250-500 m, (b) 500-1000 m, and (c) 1000-1500 m. The best-fit slopes are denoted by the red and blue solid line.

4. Summary and Discussion

The spatial pattern and seasonal variability of the diapycnal diffusivities in the Philippine Sea were estimated using a fine scale parameterization. The main conclusions are as follows.



400 The seasonal fluctuations of mixing in this area were zonally dependent. Seasonal variability was
401 strong in winter and weak in summer at mid-latitudes, with the seasonal fluctuations more obvious in
402 the upper ocean. This was attributed to the Westerlies, and the wind plays a more significant role in
403 turbulent mixing here. However, the seasonal cycle of mixing in the low latitudes was not obvious,
404 indicating that the wind-driven mixing was not dominant here. As opposed to wind-driven mixing, tidal
405 mixing was more significant in the deeper ocean.

406 Evidence that the mixing was modulated by internal tides was seen in regions of both high and low
407 eddy kinetic energy, and it was more significant with high eddy kinetic energy. The presence of high
408 eddy kinetic energy enhanced the response of K_z to internal tides, especially for the M_2 internal tide.
409 The increased rate of K_z with internal tides in the high EKE field was higher than that in the weak
410 EKE field. The existence of mesoscale features changed the vertical structure of internal tides, and
411 transferred the internal tides energy from low modes to higher modes. It was more likely to cause
412 internal tide breaking (Dunphy and Lamb 2014). The enhancement by mesoscale motions to tidal
413 mixing was more significant for M_2 internal tides. Anticyclonic eddies were more likely to increase
414 tidal mixing in the upper ocean. While the influence of cyclonic eddies to tidal mixing was slightly
415 higher than that of anticyclonic ones in the deep ocean.

416 There are several mechanisms that might explain the elevated tidal mixing in the presence of energetic
417 mesoscale environment. The vertical scales of internal tide can be reduced and the energy of internal
418 tide can be amplified near the surface in the presence of energetic mesoscale features. When internal
419 tide passes through mesoscale eddy, the energy of mode-1 internal tide can be refracted and transmitted
420 to higher-mode waves (eg. Ferrari and Wunsch, 2008, Henning and Vallis, 2004). The eddy flows can
421 also directly increase vertical shear and subsequently internal tide energy dissipation rate (eg.
422 Chavanne et al., 2010, Dunphy, 2014). The anticyclones induce higher tidal mixing than do cyclones
423 probably because of the Chimney effects associated with distinct vorticities (Jing and Wu, 2011).

424 This paper explores the modulation of the mesoscale environments on tide-induced mixing
425 statistically by some observed datasets. Theoretical clarification of the driving mechanisms is needed.
426 Some previous numerical studies can explain our conclusion to some extent. However, how and to
427 which extent the vorticity alter internal tide evolution and induced mixing have not been clearly
428 explained in theory. Moreover, the latitude range from 9°N to 36°N are discussed in this work due to
429 the limitation of fine scale parameterization method in equatorial areas. The influence of the equatorial



background flows on ocean mixing remains to be solved.

Code and data availability. The ARGO data (<ftp://ftp.argo.org.cn/pub/ARGO/global/>) set were made available by China Argo Real-time Data Center (Li Zhaoqin et al., 2019). The near surface 10 m wind speed was product by ERA-Interim dataset (<https://www.ecmwf.int/en/forecasts/datasets>). The geostrophic velocity were taken from the AVISO (<http://www.aviso.altimetry.fr/duacs/>). The internal tidal conversion rate was provided by SEANOE (<https://www.seanoe.org/data/>, C.de Lavergne et al., 2019). The corresponding data and codes are available on request to Zhenhua Xu by email.

Author contribution. The concept of this study was developed by Zhenhua Xu and extended upon by all involved. Jia You implemented the study and performed the analysis with guidance from Zhenhua Xu, Qun Li and Robin Robertson. Peiwen Zhang and Baoshu Yin collaborated in discussing the results and composing the manuscript.

Competing interests. The authors declare that they have no conflict of interest.

Acknowledgment. Funding for this study was provided by the Strategic Priority Research Program of Chinese Academy of Sciences (No.XDB42000000, XDA11010204), the National Key Research and Development Program of China (No. 2016YFC1402705, 2017YFA0604102), the National Natural Science Foundation of China (91858103, 41676006), Key Research Program of Frontier Sciences, CAS.

References

- Alford, M. H., and Gregg, M. C.: Near-inertial mixing: Modulation of shear, strain and microstructure at low latitude, *J. Geophys. Res.*, 106(C8), 16947– 16968, 2001.
- Alford, M. H.: Improved global maps and 54-year history of wind-work on ocean inertial motions. *Geophys. Res. Lett.*, 30,1424, 2003.
- Alford, M. H., MacKinnon, J. A., Simmons, H. L. & Nash, J. D.: Near-inertial internal gravity waves in the ocean. *Annu. Rev. Mar. Sci.* 8, 95–123, 2016.
- Ansong, J.K., B.K. Arbic, H.L. Simmons, M.H. Alford, M.C. Buijsman, P.G. Timko, J.G. Richman, J.F. Shriver, and A.J. Wallcraft: Geographical Distribution of Diurnal and Semidiurnal Parametric Subharmonic Instability in a Global Ocean Circulation Model. *J. Phys. Oceanogr.*, 48, 1409–1431, 2018.



- 462 Cao, Anzhou & Guo, Zheng & Song, Jinbao & Lv, Xianqing & He, Hailun & Fan, Wei. (2018).
 463 Near-Inertial Waves and Their Underlying Mechanisms Based on the South China Sea Internal
 464 Wave Experiment (2010-2011). *Journal of Geophysical Research: Oceans*. 123.
 465 10.1029/2018JC013753.
- 466 Chang, H., Xu, Z., Yin, B., Hou, Y., Liu, Y., Li, D., et al.: Generation and propagation of M2 internal
 467 tides modulated by the Kuroshio northeast of Taiwan. *Journal of Geophysical Research: Oceans*,
 468 124, 2728 – 2749, 2019.
- 469 Chavanne, C., Flament, P., Luther, D., & Gurgel, K. W.: The surface expression of semidiurnal internal
 470 tides near a strong source at Hawaii. Part II: interactions with mesoscale currents*. *JOURNAL OF*
 471 *PHYSICAL OCEANOGRAPHY*, 40(6), 1180-1200, 2010.
- 472 Deepwell, D., Stastna, M., Carr, M., and Davis, P. A., (2017), Interaction of a mode-2 internal solitary
 473 wave with narrow isolated topography, *Physics of Fluids*, 29, 076601. [https://doi.org/10.1063/1.499](https://doi.org/10.1063/1.4994590)
 474 4590
- 475 Dong, J., R. Robertson, C. Dong, P. S. Hartlipp, T. Zhou, Z. Shao, W. Lin, M. Zhou, and J. Chen:
 476 Impacts of mesoscale currents on the diurnal critical latitude dependence of internal tides: A
 477 numerical experiment based on Barcoo Seamount, *J. Geophys. Res. Oceans*, 2019.
- 478 Dunphy, M., and K. G. Lamb: Focusing and vertical mode scattering of the first mode internal tide by
 479 mesoscale eddy interaction. *J. Geophys. Res. Oceans*, 119, 523–536, 2014.
- 480 Egbert, G. D., and R. D. Ray: Estimates of M2 tidal energy dissipation from TOPEX/Poseidon
 481 altimeter data. *J. Geophys. Res.*, 106, 22 475–22 502, 2001.
- 482 Fer, I., Skogseth, R., & Geyer, F.: Internal waves and mixing in the marginal ice zone near the yermak
 483 plateau *. *Journal of Physical Oceanography*, 40(7), 1613-1630, 2010.
- 484 Ferrari, R., and C. Wunsch: Ocean circulation kinetic energy: Reservoirs, sources, and sinks. *Annu.*
 485 *Rev. FluidMech.*, 41, 253, 2009.
- 486 Grimshaw, R., Pelinovsky, E., Talipova, T., & Kurkina, O.: Internal solitary waves: propagation, defor-
 487 mation and disintegration. *Nonlinear Processes in Geophysics*, 17(6), 633-649.
- 488 Huang, X., Wang, Z., Zhang, Z., Yang, Y., Zhou, C., & Yang, Q., et al.: Role of mesoscale eddies in
 489 modulating the semidiurnal internal tide: observation results in the northern south china
 490 sea. *Journal of Physical Oceanography*, 48(8), 1749-1770, 2018.
- 491 Jayne, S. R., and L. C. St. Laurent: Parameterizing tidal dissipation over rough topography. *Geophys.*
 492 *Res. Lett.*, 28, 811–814, 2001.
- 493 Jing, Z., Wu, L., Li, L., Liu, C., Liang, X., & Chen, Z., et al.: Turbulent diapycnal mixing in the
 494 subtropical northwestern pacific: spatial-seasonal variations and role of eddies. *Journal of*
 495 *Geophysical Research Oceans*, 116., 2011.
- 496 Kerry, C. G., Powell, B. S., & Carter, G. S.: Effects of remote generation sites on model estimates
 497 of M2 internal tides in the Philippine Sea. *Journal of Physical Oceanography*, 43(1), 187 – 204,
 498 2013.
- 499 Kerry, C.G., B.S. Powell, and G. S. Carter: The impact of subtidal circulation on internal tide
 500 generation and propagation in the Philippine Sea. *J. Phys. Oceanogr.*, 44, 1386–1405, 2014.
- 501 Kerry, C. G., Powell, B. S., & Carter, G. S.: Quantifying the incoherent m 2 internal tide in the
 502 Philippine sea. *Journal of Physical Oceanography*, 46(8), 2483-2491, 2016.
- 503 Klymak, J.M., J.N. Moum, J.D. Nash, E. Kunze, J.B. Girton, G.S. Carter, C.M. Lee, T.B. Sanford, and
 504 M.C. Gregg: An Estimate of Tidal Energy Lost to Turbulence at the Hawaiian Ridge. *J. Phys.*
 505 *Oceanogr.*, 36, 1148–1164, 2006.



- 506 Kunze, E.: Internal-wave-driven mixing: global geography and budgets. *Journal of Physical*
 507 *Oceanography*, JPO-D-16-0141.1, 2017.
- 508 Liu A K, Su F C, Hsu M K et al.: Generation and evolution of mode-two internal waves in the South
 509 China Sea. *Cont. Shelf Res.*, 59:18-27, <http://dx.doi.org/10.1016/j.csr.2013.02.009>, 2013.
- 510 Liu, G., W. Perrie, and C. Hughes: Surface wave effects on the wind-power input to mixed layer
 511 near-inertial motions. *J. Phys. Oceanogr.*, 47, 1077–1093, 2017.
- 512 Li Zhaoqin, Liu Zenghong, Xing Xiaogang: User Manual for Global Argo Observational data set (V3.0)
 513 (1997–2019), China Argo Real-time Data Center, Hangzhou, 37pp, 2019.
- 514 MacKinnon, J. A. et al.: Climate process team on internal-wave driven ocean mixing. *Bull. Am.*
 515 *Meteorol. Soc.* 98, 2429–2454, 2017.
- 516 Munk, W., and C. Wunsch: Abyssal recipes II: Energetics of tidal and wind mixing. *Deep-Sea Res. I*,
 517 45, 1977–2010, 1998.
- 518 Muller, M.: On the space - and time - dependence of barotropic - to - baroclinic tidal energy
 519 conversion. *Ocean Modelling*, 72, 242 – 252, 2013.
- 520 Nagasawa, M., Hibiya, T., Furuichi, N. et al.: Temporal Variability of High Vertical Wavenumber Shear
 521 over the Izu-Ogasawara Ridge. *J Oceanogr* 61, 1101–1105, 2005.
- 522 Nash, J. D., E. L. Shroyer, S. M. Kelly, and M. E. Inall: Are any coastal internal tides predictable?
 523 *Oceanography*, 25 (2), 80–95, 2012.
- 524 Park, J.-H., and D. R. Watts: Internal tides in the southwestern Japan/East Sea. *J. Phys. Oceanogr.*, 36,
 525 22–34, 2006.
- 526 Ponte, A. L., and P. Klein: Incoherent signature of internal tides on sea level in idealized numerical
 527 simulations. *1769Geophys. Res. Lett.*, 42, 1520–1526, 2015.
- 528 Qiu, B., Chen, S., and Carter, G. S.: Time-varying parametric subharmonic instability from repeat CTD
 529 surveys in the northwestern Pacific Ocean, *J. Geophys. Res.*, 117, C09012, 2012.
- 530 Rainville, L., & Pinkel, R.: Propagation of low-mode internal waves through the ocean. *Journal of*
 531 *Physical Oceanography*, 36(6), p.1220-1236, 2006.
- 532 Rimac, A., J.-S. von Storch, C. Eden, and H. Haak: The influence of high resolution wind stress field
 533 on the power input to near-inertial motions in the ocean. *Geophys. Res. Lett.*, 40,4882–4886 ,
 534 2013.
- 535 Robertson, R.: Internal tides and baroclinicity in the southern Weddell Sea: 1. Model description.
 536 *Journal of Geophysical Research*, 27001-27016, <https://doi.org/10.1029/2000JC000475>, 2001.
- 537 Robertson, R., and C M. Dong: An evaluation of the performance of vertical mixing parameterizations
 538 for tidal mixing in the Regional Ocean Modeling System (ROMS), *Geoscience Letters*, 6 (15),
 539 2019.
- 540 Shen, H., Perrie, W., & Johnson, C. L.: Predicting internal solitary waves in the gulf of maine. *Journal*
 541 *of Geophysical Research: Oceans*, 125(3), 2020.
- 542 Song, P., and X. Chen.: Investigation of the Internal Tides in the Northwest Pacific Ocean Considering t
 543 he Background Circulation and Stratification. *J. Phys. Oceanogr.*, 50, 3165–3188,
 544 2020. <https://doi.org/10.1175/JPO-D-19-0177.1>.
- 545 Tanaka, T., Hasegawa, D., Yasuda, I., Tsuji, H., Fujio, S., & Goto, Y., et al.: Enhanced vertical turbulent
 546 nitrate flux in the kuroshio across the izu ridge. *Journal of Oceanography*, 1-9, 2018.
- 547 Vlasenko, V., Stashchuk, N., Palmer, M. R., & Inall, M. E.: Generation of baroclinic tides over an
 548 isolated underwater bank. *Journal of Geophysical Research Oceans*, 118(9), 2013.
 549 <https://doi.org/10.1002/jgrc.20304>



- 550 Watanabe, M., and T. Hibiya: Global estimates of the wind induced energy flux to inertial motions in
 551 the surface mixed layer. *Geophys. Res. Lett.*, 29, 1239, 2002.
- 552 Wang, Y., Xu, Z., Yin, B., Hou, Y., & Chang, H.: Long-range radiation and interference pattern of
 553 multisource M2 internal tides in the Philippine Sea. *Journal of Geophysical Research: Oceans*, 123, 5091–5112, 2018.
- 554 Waterhouse, A.F., J.A. MacKinnon, J.D. Nash, M.H. Alford, E. Kunze, H.L. Simmons, K.L. Polzin,
 555 L.C. St. Laurent, O.M. Sun, R. Pinkel, L.D. Talley, C.B. Whalen, T.N. Huussen, G.S. Carter, I. Fer,
 556 S. Waterman, A.C. Naveira Garabato, T.B. Sanford, and C.M. Lee: Global Patterns of Diapycnal
 557 Mixing from Measurements of the Turbulent Dissipation Rate. *J. Phys. Oceanogr.*, 44, 1854–1872,
 558 2014.
- 559 Whalen, C. B., Talley, L. D., & Mackinnon, J. A.: Spatial and temporal variability of global ocean
 560 mixing inferred from ARGO profiles. *Geophysical Research Letters*, 39(18), 2012.
- 561 Whalen, C.B., MacKinnon, J.A. & Talley, L.D.: Large-scale impacts of the mesoscale environment on
 562 mixing from wind-driven internal waves. *Nature Geosci* 11, 842–847, 2018.
- 563 Wunsch, C., and R. Ferrari: Vertical mixing, energy and the general circulation of the oceans. *Annu.*
 564 *Rev. Fluid Mech.*, 36, 281–314, 2004.
- 565 Zhang, Z., Qiu, B., Tian, J. et al.: Latitude-dependent finescale turbulent shear generations in the
 566 Pacific tropical-extratropical upper ocean. *Nat Commun* 9, 4086, 2018.
- 567 Zhao, Z., M. H. Alford, J. A. MacKinnon, and R. Pinkel: Long-range propagation of the semidiurnal
 568 internal tide from the Hawaiian Ridge. *J. Phys. Oceanogr.*, 40, 713–736, 2010.
- 569
- 570